

A Nanoscale Plasma Etching Process for Pole Tip Recession of Perpendicular Recording Magnetic Head

Shoubin LIU*, Dayao HE

School of Mechanical Engineering and Automation, Harbin Institute of Technology Shenzhen Graduate School, Shenzhen University Town, Xili, Shenzhen, 518055, China

crossref <http://dx.doi.org/10.5755/j01.ms.22.2.12953>

Received 22 August 2015; accepted 19 February 2016

The pole tip of perpendicular recording head is constructed in a stacked structure with materials of NiCoFe, NiFe, Al₂O₃ and AlTiC. The surfaces of different materials are set at different heights below the air-bearing surface of slider. This paper presented a plasma dry etching process for Pole Tip Recession (PTR) based on an ion beam etching system. Ar and O₂ mixed plasma at small incident angles have a high removal rate to the nonmagnetic material. It was utilised to etch the reference surface until it reaches the MT value. Low-energy Ar plasma at a small incident angle removes materials with selective ratios of 1 : 1.6 : 2.5 : 2.9 (AlTiC/Al₂O₃/NiCoFe/NiFe). It was selected to form the PTR. High-energy Ar plasma at a large incident angle exhibits almost same removal rates for all materials. It was adopted to make overall removal while keeping the recessed profile. An atomic force microscope (AFM) was used for measuring the recessed heights of pole tip and the MT value of the base surface. A transmission electronic microscopy (TEM) was chosen to examine the thickness of subsurface damage. A batch of production showed that the recessed heights can be successfully nanofabricated with the three-step plasma etching process.

Keywords: pole tip recession, plasma etching, selectivity, removal rate, ion damage.

1. INTRODUCTION

The pole tip of perpendicular recording magnetic head in a hard disk drive (HDD) is constructed in a stacked structure with materials of NiCoFe, NiFe, Al₂O₃ and AlTiC. It is located at the front position of the head slider, as shown in Fig. 1 a. The flying height from the pole tip to the disk surface is less than 10 nm. With a small flying height and a perpendicular magnetic recording technique, this kind of pole tips result in a very high areal density [1, 2]. To prevent contact damage with a disk, surfaces of different materials are set at different heights of several nanometers below the air-bearing surface of slider, as shown in Fig. 1 b. The recessed topology is referred to as Pole Tip Recession (PTR) [3–5].

Mechanical polishing, chemically mechanical polishing and plasma etching are three typical methods for PTR [6]. Mechanical or chemically mechanical polishing belongs to a kind of wet polishing techniques, and there is damage in some degree to pole tip materials if chemical solvent is used. The recessed heights are difficult to control because the selectivity of removal rates to different materials is influenced by lapping pressure. Consequently, mechanical or chemically mechanical process cannot be applied in the final stage of PTR. Plasma etching is a promising one especially for plasma dry etching because there is no processing force during etching [7, 8]. Many studies have been carried out theoretically or experimentally on plasma etching [9–15]. At present, plasma etching is still facing some difficulties before use, for example, the selection of ion energy, controlling etch

selectivity of different materials and acceptable etch uniformity.

In this paper, we adopted an ICP-type high-density ion beam etching system to generate Ar plasma, or Ar and O₂ mixed plasma for nanofabrication of PTR. We first identified the selective effects of etching rates under different ion incident energy and different ion incident angles on different materials of pole tip. Then we designed a three-step plasma etching process to form the recessed nanostructure of pole tip. Finally, a batch of pole tips was etched for verification of the plasma etching process.

2. EXPERIMENTAL METHODS

2.1. The materials and recessed heights of pole tip

Fig. 1 b shows the stacked structure and material composition of a pole tip, where WS is the writing region or writing pole, SF is the reading region or reading pole, OC is the overcoat for insulating, AlTiC (Al₂O₃-TiC) is the head base material. The material composition of WS is NiCoFe (83, 1, 16 wt.%), SF is NiFe (83, 17 wt.%). WS and SF are magnetic material. AlTiC and Al₂O₃ are nonmagnetic material.

AlTiC surface is also referred as reference surface. It forms the air-bearing surface (ABS) of slider after coating with diamond-like carbon (DLC) films. MT is an important parameter to describe the micro texture of AlTiC surface. As shown in Fig. 4 a and Fig. 10 a, AlTiC surface after etching is a composite of Al₂O₃ and TiO_x, showing two statistical peaks in height. The MT value refers to the difference in height of two statistical peaks of two materials. Because MT influences the flying status of slider, the base surface of AlTiC is qualified with MT.

* Corresponding author. Tel.: +86-755-26033516; fax.: +86-755-26033774. E-mail: mesbliu@hitsz.edu.cn (S. Liu)

Targets of plasma etching for PTR are, in achieving, $H_{OC} = -3.5 \pm 1$ nm (OC recession), $H_{WS} = -0.8 \pm 0.5$ nm (WS recession), $H_{SF} = -1.6 \pm 0.5$ nm (SF recession), and $MT = 1.8 \pm 0.2$ nm (ABS protrusion), while minus sign (-) means height of material is lower than the reference surface and positive sign (+) means height of material is higher than the reference surface. The etched area was controlled within $30 \mu\text{m} \times 60 \mu\text{m}$.

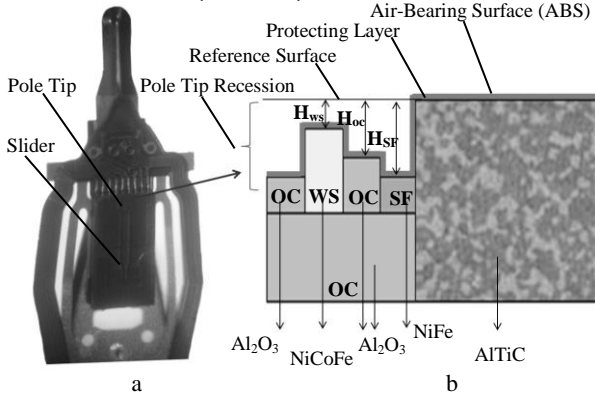


Fig. 1. a—a slider of perpendicular recording magnetic head; b—pole tip with recessed topology

2.2. The ion beam etching system

Fig. 2 shows a schematic of the ion beam etching system. It belongs to an ICP-type high-density plasma etching system [8]. The vacuum chamber of the system consists of a plasma generator, a plasma accelerating device, and a substrate holder. The plasma generator is a 13.56 MHz inductively RF coupled plasma source. When the pressure of vacuum chamber reaches the base pressure (less than 10^{-5} Pa), Ar gas and O_2 gas are supplied. Once the pressure is stabilised at 10^{-1} Pa, RF power is supplied and the plasma neutraliser is turned on gradually. High-density plasma is then generated. The accelerating device includes three grids, namely accelerating grid (anode), inhibiting grid (cathode), and grounding grid. Plasma consists of a large number of electrons and ions at high-speed. When they pass the first grid, most of the electrons are absorbed and ions go through. After ions pass the second grid, they are accelerated quickly by the electric field while electrons are restricted. The remainder of electrons is further absorbed by the third grid. Finally, the plasma gains high energy, high density, good uniformity and good stability after passing through the accelerating device, and strikes the surface of substrate. The substrate holder is a rotating platform whose speed can be regulated. The processing volume is $\Phi 20 \text{ cm} \times 2 \text{ cm}$.

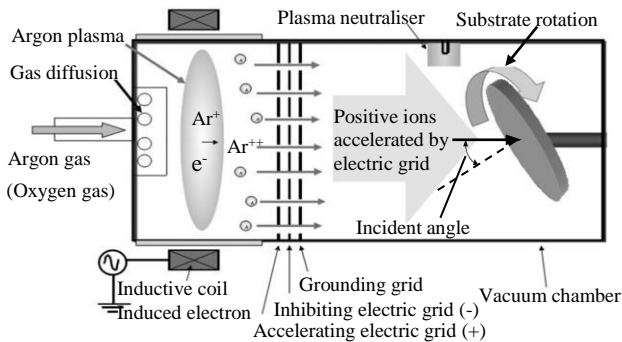


Fig. 2. A high-density ion beam etching system

As shown in Fig. 2, the incident ray of plasma forms an angle with the normal of substrate surface. This angle is named as incident angle. More precisely, incident angle refers to the angle between an incident ray of plasma and the normal of substrate surface.

2.3. Experimental procedure

To find characteristics of plasma etching of elementary materials of pole tip, we designed the experiment as follows.

Experiment 1. We used a mixture of Ar and O_2 plasma to identify the influence of ion incident angles on etching rate and MT. Experiment parameters were RF power = 130 W, anode voltage = 300 V, cathode voltage = -400 V, etching time = 6.5 min, Ar: O_2 = 15:3, flow rate of Ar = 15 sccm (standard cubic centimeter per minute, sccm), flow rate of O_2 = 3 sccm, working pressure = 0.1 Pa.

Experiment 2. We used low-energy Ar plasma to investigate the influence of ion incident angles on etching rate and MT. Experiment parameters were RF power = 105 W, anode voltage = 285 V, cathode voltage = -400 V, etching time = 6.5 min, flow rate of Ar = 18 sccm, working pressure = 0.1 Pa.

Experiment 3. We used high-energy Ar plasma to find the influence of ion incident angles on etching rate and MT. Experiment parameters were RF power = 150 W, anode voltage = 285 V, cathode voltage = -400 V, etching time = 6.5 min, flow rate of Ar = 18 sccm, working pressure = 0.1 Pa.

Experiment 4. We used high-energy Ar plasma to find damage depth in the subsurface of pole tip profile. Experiment parameters were RF power = 180 W, anode voltage = 200 V–500 V, cathode voltage = -200 V, etching time = 80 sec, flow rate of Ar = 18 sccm, working pressure = 0.1 Pa. After etching, surfaces of pole tip were coated with a layer of DLC film of 4 nm in thickness to prevent the substrate from oxidative corrosion. The DLC film was deposited by using a filtered cathodic vacuum arc (FCVA) physical vapor deposition (PVD) method.

Experiment 5. We etched a batch of pole tips with a three-step plasma etching process. The parameters adopted by each step, as detailed above, were shown in Table 1. We checked the recessed heights and MT value with an AFM for PTR process verification.

In above experiments, the etching rate can be measured with a substrate consisting of a protective zone and a non-protective zone. By etching the substrate within given time and measuring the step height of two zones with an AFM, etching rate is calculated as a ratio of step height to given time.

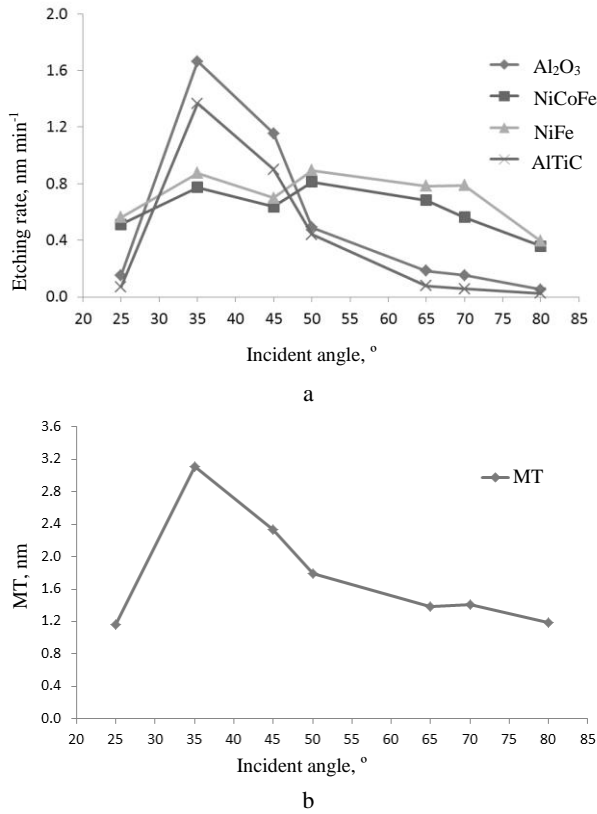
3. RESULTS AND DISCUSSION

3.1. Etching rate and MT in different incident angles of Ar and O_2 mixed plasma

Fig. 3 shows the dependence of etching rates on the incident angles in the condition of using Ar and O_2 mixed plasma. When the incident angle is in the range of 30° to 50° , the etching rates of magnetic material, NiCoFe and NiFe are changed very little. Their etching rates remain at about 0.8 nm min^{-1} .

Table 1. Three-step etching process for PTR

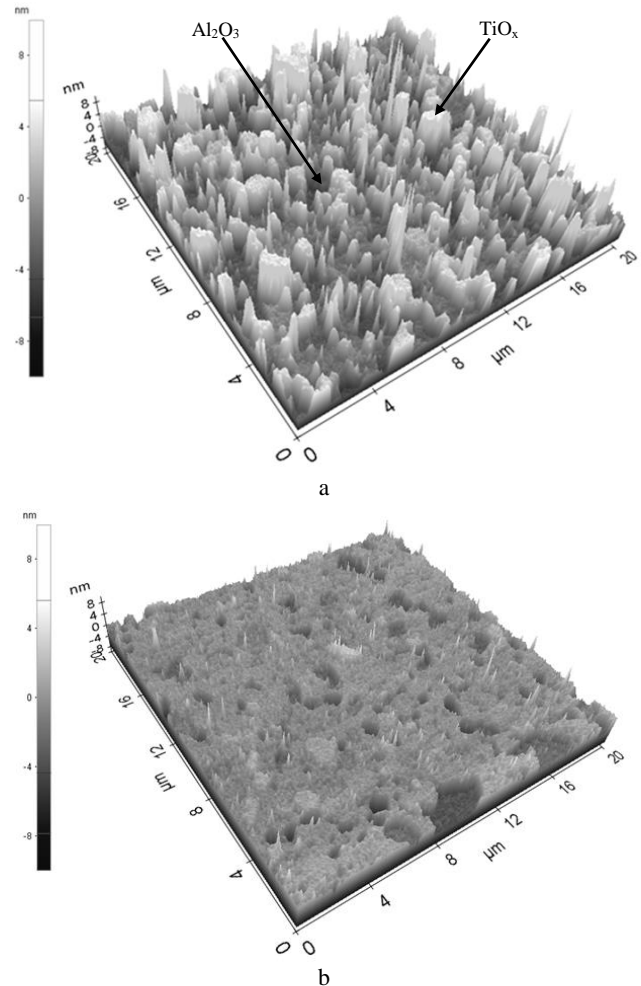
Step	RF power, W	Grid bias, V		Incident angle, °	Pallet speed, rpm	Etch time, min	Gas flow rate, sccm	
		Anode	Cathode				Ar	O ₂
Step1	145	316	-400	30	16	6.7	15	3
Step2	105	220	-550	35	16	5.0	18	0
Step3	150	285	-400	70	16	2.0	18	0

**Fig. 3.** Etching rates of four materials vary with incident angle (a), and MT of base surface varies with incident angle (b) in a condition of Ar and O₂ mixed plasma

Etching rates of nonmagnetic material, Al₂O₃ and AlTiC are greater than that of magnetic material. Their etching rates increase first and then decrease with the increase of incident angle. The etching rate of Al₂O₃ is greater than that of AlTiC. When the incident angle is 35°, etching rates of Al₂O₃ and AlTiC reach their maximum values. Fig. 3 b indicates the trend of MT as first increasing and then decreasing with the increase of incident angle. When the incident angle is 35°, MT reaches its maximum.

These effects could be explained as follows. In the condition of using Ar and O₂ mixed plasma, the etching process is a combination of ion sputtering and ion assist chemical reaction. The former is referred as physical etching, and the latter is referred as chemical etching. In general, physical etching plays an important role to overall trends of etching rates and MT values because Ar gas is dominant in the gas mixture of Ar and O₂. The incident energy of Ar and O₂ mixed plasma will release in a form of surface diffusion at a big incident angle, or dissipate by ion implantation at a small incident angle. These result in low etching rates and small MT values at two ends of Fig. 3 a and b. When the incident angle reaches a value around 35°,

sputtering by Ar and O₂ mixed plasma and chemical etching by O₂ plasma will enhance the removal rates to all materials. For magnetic material of NiCoFe and NiFe, ion sputtering is suppressed by the oxides between NiCoFe or NiFe and O₂. This results in a non-obvious increase of removal rate of magnetic material. For Al₂O₃ material, negative charge will accumulate on its surface because of its insulating property. Local high-energy plasma is thus generated and results in a high removal rate of Al₂O₃. For AlTiC material, there is no negative charge accumulation on TiC surface because TiC is a conductive material. The removal rate of TiC is thus lower than that of Al₂O₃. In the same time, O₂ plasma reacts chemically with material elements of Al, C and Ti. TiC is further oxidised as TiO_x forming the protrusion morphology of AlTiC surface. Fig. 4 shows that the MT value of micro texture at the incident angle of 35° is significantly greater than that at 85°.

**Fig. 4.** Micro texture etched at incident angle: a-35°; b-85°

As a result of Experiment 1, Ar and O₂ mixed plasma

at incident angles around 30° can be used to fabricate the surface morphology of AlTiC with a high removal rate, until it reaches the MT value. This is a coarse stage of PTR nanofabrication.

3.2. Etching rate and MT in different incident angles of low-energy Ar plasma

Fig. 5 a shows the dependence of etching rates on the incident angles in the condition of using low-energy Ar plasma. In general, etching rates of all materials are relative low. Etching rates increase first and then decrease with the increase of incident angle. This phenomenon is caused by physical collisions between atoms of materials and Ar plasma. When the incident angle is too big, the energy of Ar plasma will release in the form of surface diffusion. The etching rates are thus low. When the incident angle is around 35° , ion sputtering effect will be enhanced and etching rates will increase. Under an incident angle of 35° , etching rates of NiFe and NiCoFe are significantly faster than that of AlTiC and Al_2O_3 . The etching rate of NiFe is the fastest one. Removal rates of four materials are different obviously, showing a selective effect with selective ratios of $1 : 1.6 : 2.5 : 2.9$ (AlTiC/ Al_2O_3 /NiCoFe/NiFe).

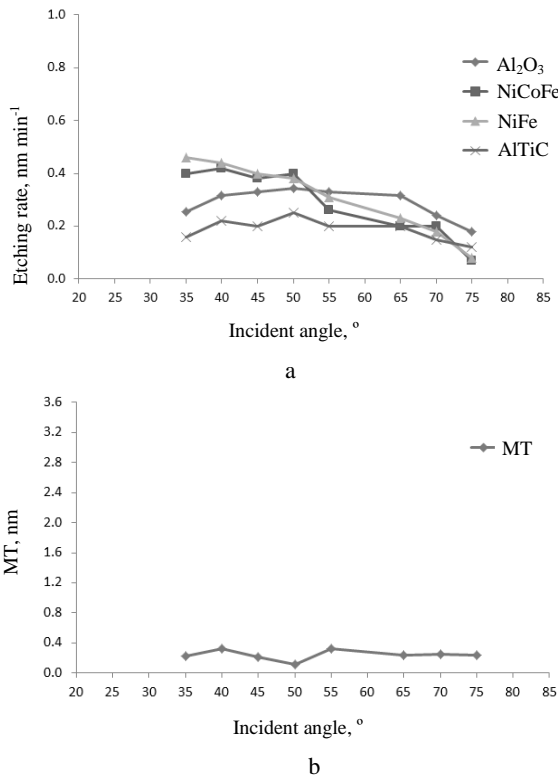


Fig. 5. Etching rates of four materials vary with incident angle (a), and MT of base surface varies with incident angle (b) in a condition of low-energy Ar plasma

Fig. 5 b indicates that MT changes non-apparently in the condition of using low-energy Ar plasma. This phenomenon is caused by the weak striking energy of Ar plasma. Due to the lack of local high-energy, entire surface of materials suffers uniform collisions. In addition, the absence of O_2 plasma results that there is no chemical reaction during etching. The chemical selectivity to material elements of C, Ti and Al in AlTiC will not appear. Therefore, in the case of low-energy Ar plasma, the

selectivity of etching rates to different material elements of AlTiC is relatively small, and MT changes inconspicuously with the change of incident angle.

As a result of Experiment 2, we can use low-energy Ar plasma at an incident angle of 35° to remove materials with selective ratios of $1 : 1.6 : 2.5 : 2.9$ (AlTiC/ Al_2O_3 /NiCoFe/NiFe) for the generation of PTR, while keeping the MT value unchanged. This is a fine stage of PTR nanofabrication.

3.3. Etching rate and MT in different incident angles of high-energy Ar plasma

Fig. 6 a shows the dependence of etching rates on the incident angles in the condition of using high-energy Ar plasma. In general, etching rates of different materials converge to similar values with the increase of incident angle. This phenomenon is caused by the physical collisions of Ar plasma. When the incident angle is small, the incident energy of Ar plasma is high. It strikes the surfaces and generates local high-energy in the sputtering direction. This results in an obvious selectivity of etching rates to different materials. While the incident angle increases continuously, the incident energy of plasma reduces dramatically. Low incident energy causes surfaces of all materials in a same excited state, and etching rates are thus reduced to small values.

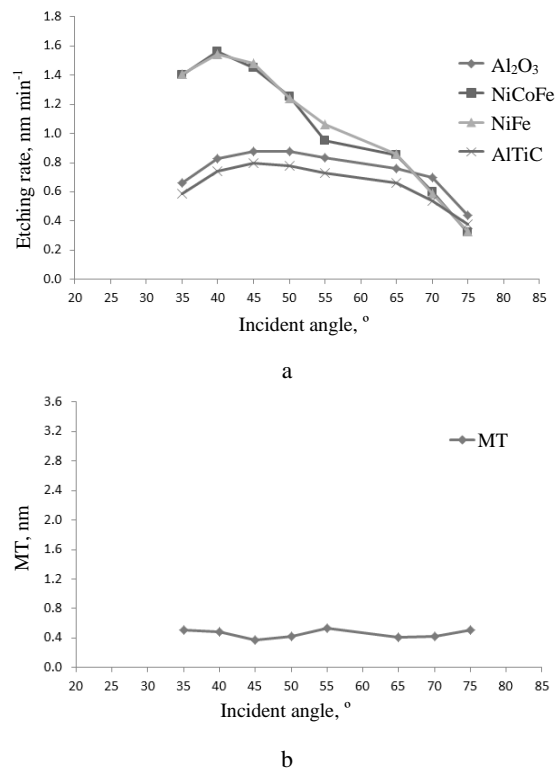


Fig. 6. Etching rates of four materials vary with incident angle (a), and MT of base surface varies with incident angle (b) in a condition of high-energy Ar plasma

When the incident angle reaches 70° , the selective effect of etching rates to different materials almost disappears, i.e. the removal rates of all materials close together. In this case, if we continue to increase etching time, the surfaces etched will overall sink while the recessed morphology is fixed.

Fig. 6 b indicates that MT shows non-obviously

changes with the increase of incident angle in the condition of using high-energy Ar plasma. The reason is that the absence of O₂ plasma results in no chemical reaction during etching. Under the striking of high-energy Ar plasma, the entire surface of AlTiC suffers uniform collisions. Therefore, the variation of etching rates to different material elements is small and MT changes non-obviously with the change of incident angle.

As a result of Experiment 3, we can use high-energy Ar plasma at a large incident angle of 70° to achieve an overall removal of surfaces of pole tip while keeping recessed morphology unchanged. With the increase of etching time, the required amount of material removal can be obtained accurately. This is a final stage of PTR nanofabrication.

3.4. The damage of subsurface of pole tip

Fig. 7 shows the effect of the grid positive bias (anode) on the thickness of damage layer of magnetic materials in the condition of using high-energy Ar plasma. While fixing the grid negative bias (cathode) as -200 V, with the increase of the grid positive bias, the thickness of damage layer of three different magnetic materials is also increased. If the grid positive bias is less than 300 V, thickness of damage layer changes smoothly. However, if the grid positive bias is greater than 300 V, thickness of damage layer increases obviously. If the grid positive bias reaches or exceeds 400 V, thickness of damage layer increases dramatically. This effect is explained by the increase of the grid positive bias leading to the increase of the plasma energy. With the grid positive bias increasing, electric field strength increases. When the ions pass through the electric field, they will be accelerated and gain more energy. Once the high-energy ions inject to the surface of a substrate, atomic lattices will be destroyed and result in subsurface damage [16, 17]. Fig. 8 shows two TEM images of damage layer of SF under the grid positive bias voltages of 200 V and 500 V.

As a result of Experiment 4, we should keep the grid positive bias less than 400 V in the final stage of etching.

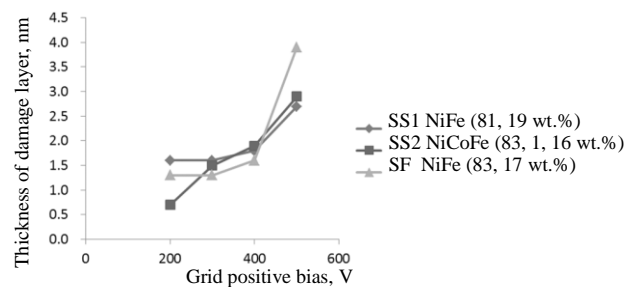


Fig. 7. The thickness of damage layer of magnetic materials varies with the grid positive bias in high-energy Ar plasma

3.5. Verification of etching process

We select 11 pieces of pole tips for verification of PTR etching process. We first use Ar and O₂ mixed plasma at an incident angle around 30° to fabricate the base surface of AlTiC. We then use low-energy Ar plasma at an incident angle of 35° to form PTR profile, and use high-energy Ar plasma at an incident angle of 70° to generate

the recessed heights of H_{OC}, H_{WS} and H_{SF}. After testing, we find that all pole tips satisfy the requirements of MT, H_{OC}, and H_{WS}. Nine pieces of pole tips satisfy the requirement of H_{SF}. Only two pieces of pole tips cannot satisfy the requirement of H_{SF}. This reminds that the uniformity of plasma density in the ion beam etching system should be optimised.

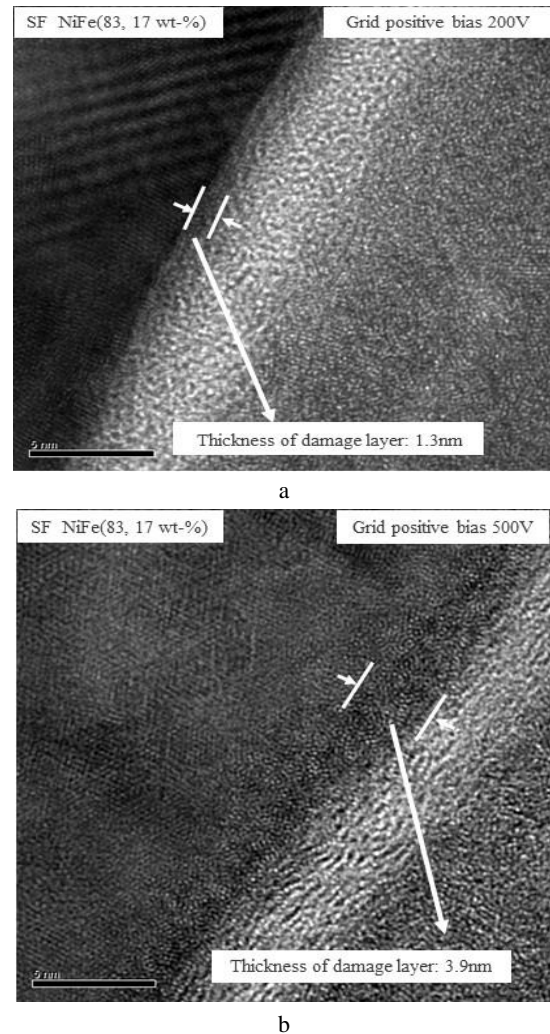


Fig. 8. TEM images showing the thickness of damage layer under grid positive bias: a - 200V; b - 500V

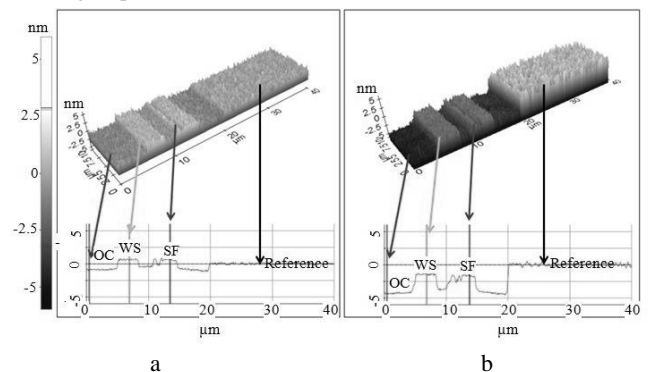


Fig. 9. AFM images of pole tip before etching (a), and after etching (b)

We add a beam mask inside the ion beam etching system to improve its uniformity. The beam mask is made of stainless steel and has a shield structure varied with the density of plasma.

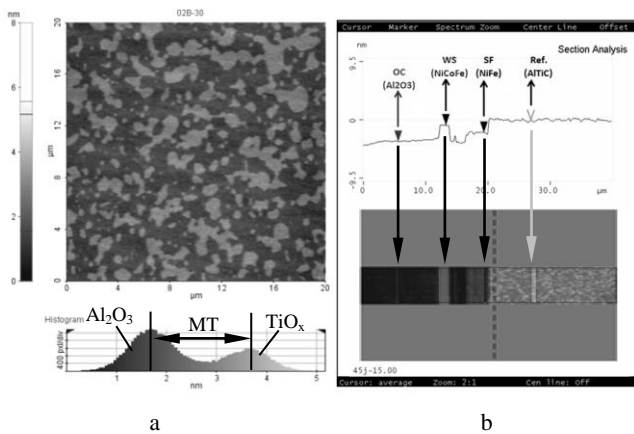


Fig. 10. a–AFM images of MT; b–recessed morphology of pole tip

The density of plasma can be measured by etching a test substrate. Through rotation of the beam mask, the uniformity of plasma density is enhanced. Another batch of pole tips is fabricated and all pole tips satisfy the requirements of MT, H_{OC} , H_{WS} , and H_{SF} . Fig. 9 shows 3D AFM images of a pole tip before and after etching. Fig. 10 shows AFM images of MT and the recessed morphology of the pole tip after etching. The three-step plasma etching process is verified successfully.

4. CONCLUSIONS

In this paper, the selectivity of removal rate of plasma etching to different materials of pole tip under different incident energy and different incident angles is well studied. A three-step plasma etching process is proposed for surface recession of pole tip of perpendicular recording magnetic head based on an ion beam etching system. In the first step, we use a mixture of Ar and O_2 plasma at incident angles around 30° to fabricate the morphology of reference surface of AlTiC with a high removal rate. In the second step, we choose low-energy Ar plasma at an incident angle of 35° to form the recessed morphology of pole tip. In the third step, we utilise high-energy Ar plasma at an incident angle of 70° to make overall removal of all materials while keeping the recessed profile unchanged. To avoid surface damage caused by high-energy plasma sputtering, the positive bias of electric grid is regulated less than 400 V. A batch of production shows that the required heights of PTR are successfully nanofabricated with the three-step plasma etching process.

REFERENCES

1. **Khizroev, S., Kryder, M., Litvinov, D.** Next Generation Perpendicular Systems *IEEE Transactions on Magnetics* 37 (4) 2001: pp. 1922–1925. <http://dx.doi.org/10.1109/20.951009>
2. **Khizroev, S., Litvinov, D.** Perpendicular Magnetic Recording: Writing Process *Journal of Applied Physics* 95 (9) 2004: pp. 4521–4537.

<http://dx.doi.org/10.1063/1.1695092>

3. **Xu, J., Bhushan, B.** Pole Tip Recession Studies of Thin-film Rigid Disk Head Sliders *Wear* 219 (1) 1998: pp. 16–29.
4. **Scott, W., Bhushan, B.** A Model of Pole Tip Recession Growth in Magnetic Heads *Journal of Applied Physics* 91 (10) 2002: pp. 8328–8330.
5. **Kwon, J., Kim, Y., Yoon, K., Lee, S., Park, S.** Advanced Nanoscale Metrology of Pole-tip Recession with AFM *Ultramicroscopy* 105 (1) 2005: pp. 51–56.
6. **Jiang, M., Hao, S., Komanduri, R.** On the Advanced Lapping Process in the Precision Finishing of Thin-film Magnetic Recording Heads for Rigid Disc Drives *Applied Physics A* 77 (7) 2003: pp. 923–932.
7. **Shohet, J.** Plasma-aided Manufacturing *IEEE Transaction Plasma Science* 19 (5) 1991: pp. 725–733. <http://dx.doi.org/10.1109/27.108405>
8. **Lieberman, M., Lichtenberg, A.** Principles of Plasma Discharges and Materials Processing, 2nd Edn, John Wiley & Sons, 2005. <http://dx.doi.org/10.1002/0471724254>
9. **Shamiryan, D., Paraschiv, V., Boullart, W., Baklanov, M.** Plasma Etching: from Micro- to Nanoelectronics *High Energy Chemistry* 43 (3) 2009: pp. 204–212.
10. **Zeniou, A., Ellinas, K., Olziersky, A., Gogolides, E.** Ultra-High Aspect Ratio Si Nanowires Fabricated with Plasma Etching: Plasma Processing, Mechanical Stability Analysis Against Adhesion and Capillary Forces and Oleophobicity *Nanotechnology* 25 (3) 2014: pp. 035302-1–035302-11.
11. **Cansizoglu, M., Karabacak, T.** Engineering Morphology of Surfaces by Oblique Angle Etching *Materials Research Society Symposium Proceedings* 1059 2008: pp. 119–124.
12. **Aizawa, T., Fukuda, T.** Oxygen Plasma Etching of Diamond-like Carbon Coated Mold-die for Micro-Texturing *Surface and Coatings Technology* 215 (4) 2013: pp. 364–368. <http://dx.doi.org/10.1016/j.surfcoat.2012.07.095>
13. **Leghrib, R., Clement, P., Llobet, E.** RF Sputtering as A Tool for Plasma Treating and Metal Decoration *Procedia Engineering* 25 (35) 2011: pp. 223–226.
14. **Tian, Y., Liu, W., Hang, L.** Influence of Oxygen Flow Rate on the Variation of Surface Roughness of Fused Silica During Plasma Polishing Process *Physics Procedia* 18 (6) 2011: pp. 107–111.
15. **Vesel, A., Mozetic, M., Panjan, P., Hauptman, N., Klanjsek-Gunde, M., Balat-Pichelin, M.** Etching of Carbon-tungsten Composite with Oxygen Plasma *Surface and Coatings Technology* 204 2010: pp. 1503–1508.
16. **Kawakami, R., Niibe, M., Takeuchi, H., Konish, M., Mori, Y., Shirahama, T., Yamada, T., Tominaga, K.** Surface Damage of 6H-SiC Originating from Argon Plasma Irradiation *Nuclear Instruments and Methods in Physics Research B* 315 (15) 2013: pp. 213–217.
17. **Wei, W., Zhu, Y., Yang, J., Yang, F.** Damage of Cr Film by Oxygen Plasma *Applied Surface Science* 301 (4) 2014: pp. 539–543.